Journal of ELECTRONIC MATERIALS, Vol. 41, No. 8, 2012
DOI: 10.1007/s11664-012-2124-4

The Effect of Crystallographic Orientation on the Mechanical Behavior of Cu_6Sn_5 by Micropillar Compression Testing

LING JIANG,[1] HANQING JIANG,[2] and NIKHILESH CHAWLA[1,2,3]

1.—Materials Science and Engineering, Arizona State University, Tempe, AZ 85287-6106, USA. 2.—Mechanical and Aerospace Engineering, Arizona State University, Tempe, AZ 85287-6106, USA. 3.—e-mail: nchawla@asu.edu

The anisotropy of the micromechanical behavior of single-crystal Cu_6Sn_5 was studied by nanoindentation and microcompression testing of pillars. Electron backscattered diffraction was employed to determine the crystallographic orientation and texture of Cu_6Sn_5 nodules. Characterization results from orientation imaging mapping show that the growth direction of the nodules is somewhat aligned to the *c*-axis of the unit cell of Cu_6Sn_5, although a fair amount of deviation exists in several grains. Normal to the growth axis the orientation is random, indicating a fiber texture. The mechanical properties indicate a 20% increase in strength and 7% increase in Young's modulus close to the *c*-axis relative to normal to the *c*-axis. Careful analysis of the results based on angle to the *c*-axis shows a linear decrease in strength with increasing deviation from the *c*-axis. Our results should help understanding and fracture modeling of Cu_6Sn_5 under thermal and mechanical loading conditions.

Key words: Crystallographic orientation, focused ion beam, micropillar compression, Cu_6Sn_5

INTRODUCTION

With the increasing focus on developing environmentally benign electronic packages, Pb-free alloys have received a great deal of attention.[1] Most Pb-free solders are Sn-rich, with slight alloying additions of Ag and/or Cu. A Cu_6Sn_5 intermetallic layer grows from the reaction between the Sn-rich liquid and Cu substrate. The thickness and morphology of this Cu_6Sn_5 intermetallic layer significantly affect the mechanical performance of the solder;[2,3] For example, a relatively thin intermetallic layer may be beneficial in achieving a strong mechanical and chemical bond between Sn and Cu substrate.[2,4] At larger thickness, however, the intermetallic often acts as a crack initiation site, leading to catastrophic failure and poor toughness of the joint.[3,5,6] Thus, fundamental understanding of the mechanical properties of Cu_6Sn_5 intermetallic is extremely important.

(Received December 27, 2011; accepted April 30, 2012; published online May 31, 2012)

Characterizing the elastic and plastic properties of the Cu-Sn intermetallics is not trivial. Bulk intermetallics have been fabricated by casting and annealing processes,[7–9] but these contain residual porosity and/or oxides. Furthermore, the intermetallic in the joint and that in bulk may differ significantly in grain size, defects, and crystallographic orientation. Indeed, preliminary studies on the Young's modulus of Cu-Sn intermetallics show a large degree of variability.[7–11] Clearly, the properties of the actual intermetallics in the joint must be evaluated. This is quite a challenge, since the intermetallic reaction layers are of the order of only a few micrometers.

Instrumented indentation has been used to obtain the Young's modulus and hardness of Cu_6Sn_5.[12–16] In our previous study,[17] we used micropillar compression as a unique means of probing the mechanical properties of this important intermetallic. Micropillars were milled using focused ion beam (FIB) within single-crystal nodules of Cu_6Sn_5, and tested in compression using a nanoindenter with a flat tip. We reported the fracture strength

and strain to failure of Cu_6Sn_5 and the effect of several parameters, such as pillar taper and aspect ratio, on micropillar compression behavior. In this study, the effect of crystallographic orientation on the mechanical behavior of Cu_6Sn_5 nodules was investigated by micropillar compression experiments. Orientation imaging mapping (OIM) was used to obtain the crystallographic orientation of individual single-crystal nodules, both parallel to the growth direction of Cu_6Sn_5 nodules (along the *c*-axis) and perpendicular to the growth direction.

EXPERIMENTAL PROCEDURES

High-purity Sn-3.9Ag-0.7Cu (SAC) ingots (Indium, Ithaca, NY) were cut into squares of approximately 6.35 mm × 6.35 mm × 1 mm. These were reflowed on oxygen-free copper bars (50.8 mm and 6.35 mm in thickness) polished to a 0.05 μm finish with colloidal silica. A graphite mask was applied to the copper bars, leaving a 6.35 mm × 6.35 mm area for reflow. A rosin mildly activated (RMA) flux was applied to improve wetting between the copper and the solder. The joint was fixed within a copper fixture, and the entire assembly was heated on a hot plate. The joints were heated to 120°C for 2 min to allow the flux to burn out, followed by melting at 220°C for 40 s. The assembly was then removed from the hot plate and air-cooled on an aluminum heat sink. After cooling to room temperature, the joint was aged at 300°C for 1 week to obtain a layer of Cu_6Sn_5 approximately 100 μm to 150 μm thick. Polished cross-sections were prepared perpendicular and parallel to the growth direction of Cu_6Sn_5. The crystallographic orientation of the samples was characterized using electron backscattered diffraction (EBSD).

A dual-beam FIB and scanning electron microscopy (SEM, Nova 200 NanoLab FEG-SEM/FIB; FEI Co., OR) were used to mill micropillars of Cu_6Sn_5 in the single-crystal Cu_6Sn_5 nodules. Initially, a beam of Ga^+ ions at current of 5 nA was used to mill out a circular trench with diameter of about 25 μm and a coarse pillar in the center with diameter of 5 μm. Then, a finer current of 30 pA was used to mill the pillar down to an average diameter of 2 μm to 3 μm. The typical aspect ratio (length/diameter) of the pillars was between 2 and 3. Several pillars in multiple grains in the joints, both parallel and perpendicular to the growth direction of Cu_6Sn_5, were fabricated. By the standard milling approach, pillars with taper angle of 4° to 8° were obtained. To minimize the taper of the pillar, the "ion-lathe" technique was used.[18] Here the sample is tilted so that the beam intersects the pillar tangentially to the surface. By repeating this process over multiple small angle increments of 10°, a pillar with taper angles of 1° to 1.5° was obtained.

The pillars were tested in compression using a commercial nanoindenter (MTS XP; Agilent Technologies, Chandler, AZ). A Berkovich indenter (three-sided pyramid; Micromaterials, Wrexham, UK) with flat triangular cross-section (10 μm on a side) was used. Experiments were performed at nominal strain rate of 0.05 s^{-1}. A continuous measurement system (CSM) was used to measure the contact stiffness instantaneously as a function of indentation depth.

For accurate measurement of the displacement of the pillar, the elastic deformation of both the diamond indenter and the bulk substrate below the pillar were subtracted. This was done by using the equation by Sneddon,[19,20] who considered the punching effect of a cylindrical punch indenting into an elastic half-space. The displacement of the pillar is then given by:

$$d_p = d_{meas} - \frac{(1-\nu_i^2)}{E_i}\left(\frac{F_{meas}}{d_t}\right) - \frac{(1-\nu_b^2)}{E_b}\left(\frac{F_{meas}}{d_b}\right), \quad (1)$$

where d_p and d_{meas} represent the displacement on the pillar and the displacement measured by the instrument, respectively. d_b is the displacement of

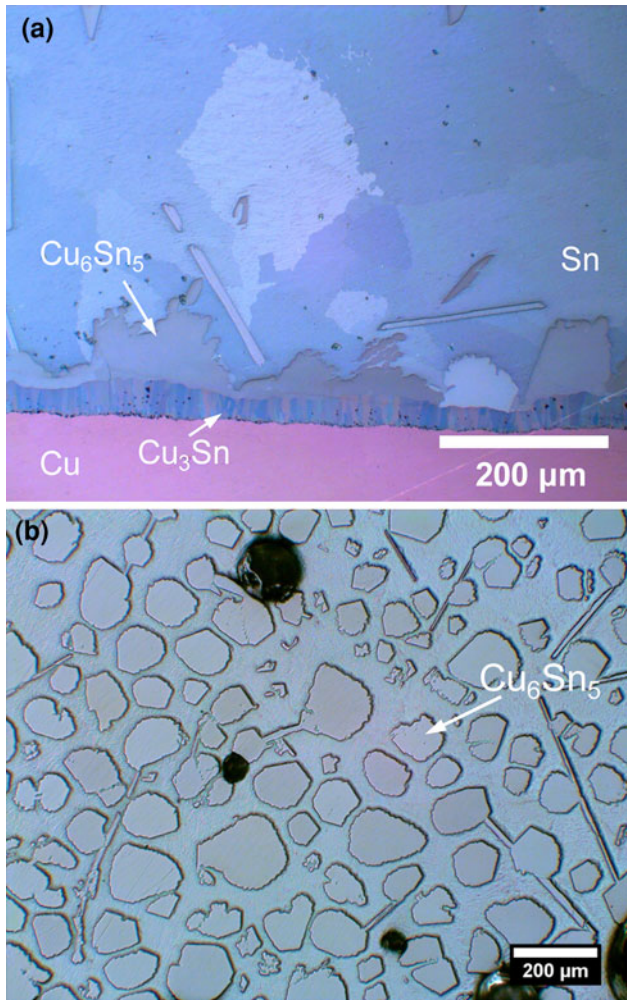

Fig. 1. (a) Optical micrograph of as-aged Sn-3.9Ag-0.7Cu/Cu solder joint polished parallel to growth axis (side view) and (b) optical micrograph of an as-aged solder joint polished perpendicular to growth direction (top view).

the base material (sink-in effect), which is also Cu_6Sn_5. F_{meas} is the measured force, E_i and υ_i are the Young's modulus and Poisson's ratio of diamond (1141 GPa and 0.07,[21] respectively), E_b is the bulk Young's modulus of Cu_6Sn_5, and υ_b is the Poisson's ratio of Cu_6Sn_5, which is taken to be 0.31.[14] In order to obtain E_b, nanoindentation with a sharp tip was carried out in the individual grains. Young's modulus values for a given indentation were taken as the average value over a specimen depth where modulus was independent of depth, i.e., approximately 200 nm to 950 nm into the specimen.

RESULTS AND DISCUSSION

The microstructure of the SAC alloy reflowed on copper is shown in Fig. 1. The sample was polished perpendicular to the growth axis of the Cu_6Sn_5 nodules, as well as parallel to the growth direction. Prior to machining pillars with the FIB, the orientation of the Cu_6Sn_5 grains was characterized by OIM. There is some controversy about the crystal structure of Cu_6Sn_5.[22,23] Our work seems to support that of Frear,[22] who showed that the structure appears to be a superlattice based on a hexagonal unit cell. Orientations of multiple grains, both along the growth axis and normal to the growth axis, were obtained. Figure 2a shows two grains parallel to the growth axis, while a view of grains normal to the growth axis is shown in Fig. 2b. The inverse pole figures of the orientation of several grains, both parallel to the growth axis (Fig. 3a) and normal to the growth direction (Fig. 3b), are shown. In general, the Cu_6Sn_5 nodules appear to grow along the *c*-axis of the unit cell, although the alignment is not perfect. A fair amount of deviation from the *c*-axis is often observed, as shown in Fig. 3b. The orientation

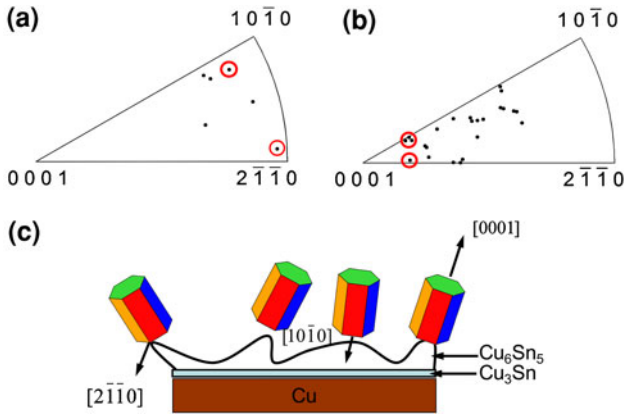

Fig. 3. Inverse pole figure maps for many Cu_6Sn_5 grains: (a) parallel to the growth direction and (b) perpendicular to the growth direction. (c) Schematic showing the orientation of the unit cells relative to growth of Cu_6Sn_5. The growth direction of all the grains is not perfectly aligned to the *c*-axis. The grains with circles indicate orientations used for pillar compression, to adequately quantify the anisotropy in mechanical properties.

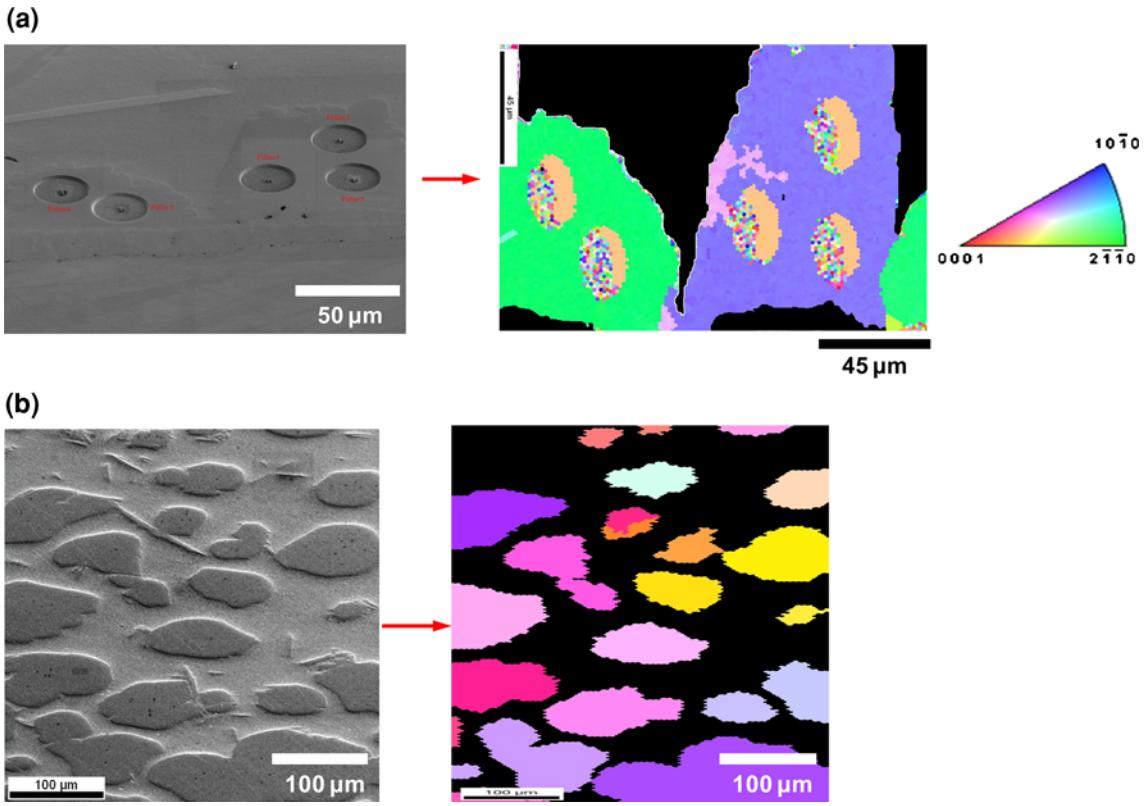

Fig. 2. SEM micrographs and orientation image maps for Cu_6Sn_5 grains: (a) parallel to the growth direction and (b) perpendicular to the growth direction.

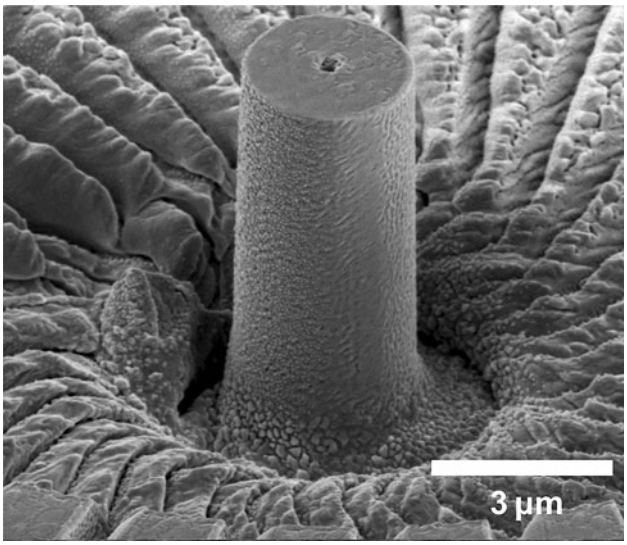

Fig. 4. A taper-free pillar fabricated using the ion-lathe technique.

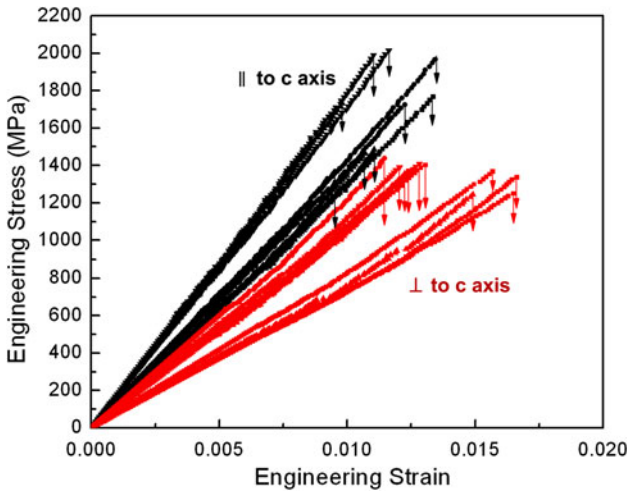

Fig. 5. Comparison of compression strength of Cu_6Sn_5 close to the *c*-axis versus perpendicular to the *c*-axis. The strength is clearly higher along the *c*-axis of Cu_6Sn_5.

normal to the growth axis is quite random, with orientations occurring between $[10\bar{1}0]$ and $[2\bar{1}\bar{1}0]$. This suggests a fiber texture in Cu_6Sn_5, as shown in Fig. 3c, with a preferred orientation closer to the *c*-axis (although not perfectly aligned to this axis) along the growth direction and random orientation normal to the growth axis. We hypothesize that the degree of alignment to the *c*-axis would be a function of growth thickness. In other words, as the Cu_6Sn_5 layer gets thicker, the orientation should be close to that of the *c*-axis. It should be noted that, as this layer gets thicker, the nodules are prone to merge together, forming a uniform and flat layer of Cu_6Sn_5.[24] At even longer aging times, Cu_3Sn can also form between Cu_6Sn_5 and Cu.

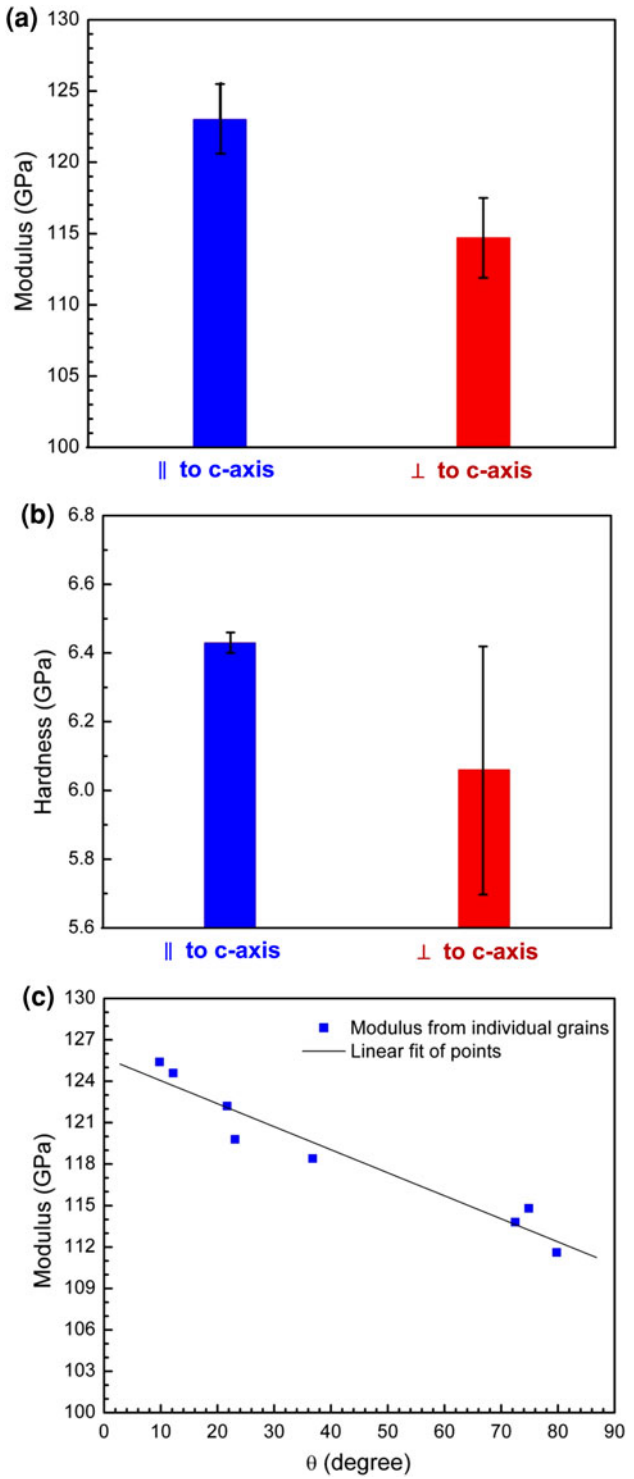

Fig. 6. (a) Comparison of Young's modulus of Cu_6Sn_5 grains compressed parallel and perpendicular to the *c*-axis, (b) similar comparison in hardness, and (c) Young's modulus of Cu_6Sn_5 grains as a function of θ (the angle between the orientation of grains and the *c*-axis of unit cell).

To investigate the effect of crystallographic orientation on the anisotropy in the mechanical behavior of Cu_6Sn_5 nodules, multiple grains were machined by FIB, normal to the growth axis and

Table I. Measurements for Young's modulus of Cu_6Sn_5 obtained by nanoindentation

IMC	Young's Modulus (GPa)	Sample Description	Remarks
Cu_6Sn_5	114.7 ± 2.8 (⊥ to *c*-axis)	Sn-3.9Ag-0.7Cu/Cu	This study
	123 ± 2.5 (|| to *c*-axis)	Joint annealed at 300°C	
	117 (parallel to (110))	Sn-1.0Ag-0.5Cu, current stressed,	Song et al.[25]
	127 (along (110))	reflowed at 400°C	
	112.3 ± 5.0	Sn-3.5Ag/Cu joint annealed at 240°C	Deng et al.[12]
	119 ± 6.0	Bulk, solid state aging of diffusion couples	Chromik et al.[13]
	114.9 ± 1.5	Bulk, casting	Jang et al.[15]
	116.3 ± 3.9	Sn-3.7Pb/Cu joint annealed at 240°C	
	125 ± 6.8	Sn-3.5Ag/Cu joint annealed at 240°C	
	116.9 ± 2.0 (perpendicular)	Bulk, solid-state aging of diffusion couples	Yang et al.[16]
	119.0 ± 1.9 (lateral)		

parallel to the growth axis. Figure 4 shows an example of a Cu_6Sn_5 pillar fabricated by FIB. The orientation of these pillars is circled in Fig. 3a, b. The idea was to obtain pillars as close to the *c*-axis as possible and to compare these with pillars with orientations normal to the *c*-axis.

The results of micropillar compression are shown in Fig. 5. Fracture of the pillar was designated as the first large discontinuity in the stress–strain curve, as per our previous work.[17] This point is relatively easy to discern because of the cleavage-like fracture observed in Cu_6Sn_5 intermetallic. Note that the pillars oriented along the *c*-axis have higher strength (1724 ± 242 MPa) than those machined normal to the growth axis (1356 ± 64 MPa). The strength close to the *c*-axis is approximately 20% higher than that normal to this axis.

Young's modulus values for individual grains were also characterized using nanoindentation with a Berkovich indenter. The average Young's modulus close to the *c*-axis was 123 ± 2.5 GPa, while that normal to the *c*-axis was 114.7 ± 2.8 GPa, as shown in Fig. 6a. This corresponds to about a 7% increase in Young's modulus along the *c*-axis. Preliminary studies on Young's modulus of Cu_6Sn_5 intermetallic using instrumented indentation show a certain degree of variability.[12,13,15,16] A comparison of our measurement results with those reported by previous studies is presented in Table I. The Young's moduli reported by previous studies fall nicely within the range of our nanoindentation measurements. Anisotropy in the modulus of Cu_6Sn_5 may be an important factor to explain the variability of Cu_6Sn_5 in the literature. Our results are consistent with those reported by Song et al.,[25] who carried out nanoindentation of Cu_6Sn_5 along the (110) axis and parallel to this axis. A comparison of anisotropy in hardness is shown in Fig. 6b. There is some anisotropy, but it is very small, since plasticity in this brittle intermetallic is limited. This finding is also corroborated by the study of Song et al.[25]

Finally, the degree of anisotropy in Young's modulus can also be quantified by examining the modulus data as a function of the angle, θ, from the *c*-axis. This direction cosine l_3, can be used to obtain the angle, θ, which is defined as the angle between the *c*-axis and the normal to the plane of interest:

$$l_3 = \cos\theta = \frac{l \cdot c*}{\sqrt{(h^2 + k^2 + hk)a*^2 + l^2c*^2}},$$

where h, k, i, and l are Bravais–Miller four-index symbols with $i = -(h + k)$; $a* = \frac{2}{a\sqrt{3}}$; $c^* = 1/c$ (a, c are parameters of the unit cell). Figure 6c shows a plot of Young's modulus versus the angle, θ. The Young's modulus decreases linearly with an increase in θ; i.e., the orientation of the grains becomes less aligned with the c-axis of the unit cell.

CONCLUSIONS

We have used micropillar compression experiments to quantify the degree of anisotropy in Young's modulus and compressive strength of Cu_6Sn_5. Characterization results from OIM show that the growth direction of the nodules is somewhat aligned to the *c*-axis of the unit cell of Cu_6Sn_5, although a fair amount of deviation exists in several grains. Normal to the growth axis the orientation is random, indicating a fiber texture. The mechanical properties indicate a 20% increase in strength and 7% increase in Young's modulus close to the *c*-axis relative to normal to the *c*-axis. Careful analysis of the results based on angle to the *c*-axis shows a linear decrease in strength with increasing deviation from the *c*-axis. Our results should help understanding and fracture modeling of Cu_6Sn_5 under thermal and mechanical loading conditions.

ACKNOWLEDGEMENTS

The authors are grateful for financial support from the Center for Engineering Materials (CEMAT) at Arizona State University. The authors thank Mr. Kenneth Mossman for assistance with EBSD.

REFERENCES

1. N. Chawla, *Int. Mater. Rev.* 54, 368 (2009).
2. P. Protsenko, A. Terlain, V. Traskine, and N. Eustathopoulos, *Scripta Mater.* 45, 1439 (2001).

3. D.R. Frear, *JOM* 48, 49 (1996).
4. Y.C. Chan, A.C.K. So, and J.K.L. Lai, *Mater. Sci. Eng. B* 55, 5 (1998).
5. D.R. Frear and P.T. Vianco, *Metall. Trans. A* 25, 1509 (1994).
6. R.E. Pratt, E.I. Stromswold, and D.J. Quesnel, *J. Electron. Mater.* 23, 375 (1994).
7. R.J. Fields, S.R. Low III, and G.K. Lucey Jr., *The Metal Science of Joining*, ed. M.J. Cieslak, J.H. Perepezko, S. Kang, and M.E. Glicksman (Warrendale, PA: TMS, 1992), p. 165.
8. B. Subrahmanyan, *Trans. Jpn. Inst. Met.* 130, 93 (1972).
9. D.R. Frear, *in Mechanics of Solder Alloy Interconnects*, eds. D.R. Frear, S.N. Burchett, and H.S. Morgan (New York: Van Nostrand Reinhold, 1994), p. 60.
10. L.M. Ostrovskaya, V.N. Rodin, A.I. Kuznetsov, and J. Soviet, *Non-ferr. Met. (Tsvetnye Metally)* 26, 90 (1985).
11. H. Rhee, J.P. Lucas, and K.N. Subramanian, *J. Mater. Sci.* 13, 477 (2002).
12. X. Deng, N. Chawla, K.K. Chawla, and M. Koopman, *Acta Mater.* 52, 4291 (2004).
13. R.R. Chromik, R.P. Vinci, S.L. Allen, and M.R. Notis, *J. Mater. Res.* 18, 2251 (2003).
14. G. Ghosh, *J. Mater. Res.* 19, 1439 (2004).
15. G.Y. Jang, J.W. Lee, and J.G. Duh, *J. Electron. Mater.* 33, 1103 (2004).
16. P.F. Yang, Y.S. Lai, S.R. Jian, J. Chen, and R.S. Chen, *Mater. Sci. Eng. A* 485, 305 (2008).
17. L. Jiang and N. Chawla, *Scripta Mater.* 63, 480 (2010).
18. M.D. Uchic and D.M. Dimiduk, *Mater. Sci. Eng. A* 400–401, 268 (2005).
19. C.A. Volkert and E.T. Lilleodden, *Philos. Mag.* 86, 5567 (2006).
20. C.P. Frick, B.G. Clark, S. Orso, A.S. Schneider, and E. Arzt, *Mater. Sci. Eng. A* 489, 319 (2008).
21. G. Simmons and H. Wang, *Single Crystal Elastic Constants and Calculated Aggregate Properties: A Handbook* (Cambridge, MA: MIT Press, 1971).
22. D.R. Frear (Ph.D. Thesis, University of California Berkeley, 1987), p. 80.
23. A.-K. Larsson, L. Stenberg, and S. Lidin, *Acta Crystallogr. B* 50, 636 (1994).
24. X. Deng, G. Piotrowski, J.J. Williams, and N. Chawla, *J. Electron. Mater.* 32, 1403 (2003).
25. J.-M. Song, B.-R. Huang, C.-Y. Liu, Y.-S. Lai, Y.-T. Chiu, and T.-W. Huang, *Mater. Sci. Eng. A* 534, 53 (2011).